

On the coherent rotation of diffuse matter in numerical simulations of galaxy clusters

Anna Silvia Baldi,^{1*} Marco De Petris,¹ Federico Sembolini,^{1,2,3}
Gustavo Yepes,^{2,3} Luca Lamagna¹ and Elena Rasia^{4,5}

¹*Dipartimento di Fisica, Sapienza Università di Roma, Piazzale Aldo Moro, 5-00185 Roma, Italy*

²*Departamento de Física Teórica, Módulo 8, Facultad de Ciencias, Universidad Autónoma de Madrid, E-28049 Cantoblanco, Madrid, Spain*

³*Astro-UAM, UAM, Unidad Asociada CSIC*

⁴*INAF, Osservatorio Astronomico di Trieste, via Tiepolo 11, I-34131 Trieste, Italy*

⁵*Department of Physics, University of Michigan, 450 Church St., Ann Arbor, MI 48109, USA*

Accepted XXX. Received YYY; in original form ZZZ

ABSTRACT

We present a study on the coherent rotation of the intracluster medium and dark matter components of simulated galaxy clusters extracted from a volume-limited sample of the MUSIC project. The set is re-simulated with three different recipes for the gas physics: (i) non-radiative, (ii) radiative without AGN feedback, and (iii) radiative with AGN feedback. Our analysis is based on the 146 most massive clusters identified as relaxed, 57 per cent of the total sample. We classify these objects as rotating and non-rotating according to the gas spin parameter, a quantity that can be related to cluster observations. We find that 4 per cent of the relaxed sample is rotating according to our criterion. By looking at the radial profiles of their specific angular momentum vector, we find that the solid body model is not a suitable description of rotational motions. The radial profiles of the velocity of the dark matter show a prevalence of the random velocity dispersion. Instead, the intracluster medium profiles are characterized by a comparable contribution from the tangential velocity and the dispersion. In general, the dark matter component dominates the dynamics of the clusters, as suggested by the correlation between its angular momentum and the gas one, and by the lack of relevant differences among the three sets of simulations.

Key words: galaxies: clusters: general – methods: numerical – cosmology: miscellaneous – cosmology: theory.

1 INTRODUCTION

The dynamics, and the rotational motions in particular, of all matter components (galaxies, diffuse gas, and dark matter) of galaxy clusters, have not been fully explored yet. This is mostly due to the complexity of these large systems and to the relatively low statistics available on their dynamical properties.

From a theoretical point of view there are some mechanisms related to structure formation that can produce coherent rotational motions of the intracluster medium (ICM) and galaxies, as well as of dark matter (DM). A first approach on the study of the origin of global angular momentum in cosmic structures was attempted by Peebles (1969), who proposed the tidal torque from surrounding matter as a possible cause of a rotation. A consequence of this interaction is a

lognormal distribution of the spin parameters of DM haloes (Catelan & Theuns 1996). An alternative mechanism that can give origin to a large-scale rotational motion is the occurrence of off-axis merging events, (Ricker 1998; Ricker & Sarazin 2001) that can be induced by tidal torque itself (Roettiger & Flores 2000).

The presence of rotational motions in clusters can affect some of their structural and evolutionary properties. The mass function derived from galaxy cluster studies is one of the most effective approaches to obtain cosmological parameters (see e.g. Vikhlinin et al. 2009; Ade et al. 2016). Its determination, however, is limited by the systematics affecting the measure of the cluster total mass. In this context, the understanding of gas motions is of fundamental importance to solve the problem of the mass bias due to the lack of hydrostatic equilibrium (see e.g. Biffi et al. 2016). Non-thermal contributions to the gas pressure, indeed, might come from turbulence, but also from coherent rotation. In Nipoti et al.

* E-mail: anna.silvia.baldi@roma1.infn.it

(2015), the effect of ICM rotation on the magneto-rotational stability in the cool core of relaxed clusters is investigated. Another process that may be influenced by a rotation of the gas is the accretion of matter onto the central cD galaxies in clusters (Tutukov, Dryomov & Dryomova 2007).

From an observational point of view, multi-wavelength techniques applied to different observables can be used for the study of the dynamics of clusters through the exploration of ICM and galaxy members. Observations are still at a primordial stage, nowadays; nevertheless some attempts to measure the rotational velocity of ICM and galaxies have been made. A method that is used to investigate rotational motions, and to possibly classify clusters as rotating, consists in checking the presence of velocity gradients in different regions of the clusters with respect to the centre. Dupke & Bregman (2001), using Doppler shift of X-ray emission lines from *ASCA* observations of the ICM in Perseus cluster, have found a velocity gradient in the outer regions which is consistent with a rotational velocity of almost 1000 km s^{-1} at 90 per cent confidence level. Recently the central regions ($r \lesssim 100 \text{ kpc}$) of the same cluster have been observed with the *Hitomi* satellite (Aharonian et al. 2016). Data reveal a gradient of the velocity projected on the line of sight of about $(150 \pm 70) \text{ km s}^{-1}$, and a velocity dispersion that is compatible with a relatively low amount of turbulent motions, suggesting a quiescent dynamics. Another recent application of X-ray spectroscopy to explore gas motions can be found in Liu et al. (2015, 2016), where *Chandra* data have been used for the study of bulk motions in disturbed clusters. Still referring to observations of the diffuse baryonic component, a coherent rotation of ICM can also be investigated in the millimetric band by observing the induced kinematic Sunyaev–Zel’dovich (SZ) contribution to cosmic microwave background temperature fluctuations. This challenging target has been explored by Cooray & Chen (2002) assuming a solid body model for a cluster, and described analytically by Chluba & Mannheim (2002). A first study on the detectability of this signal is reported in Sunyaev, Norman & Bryan (2003), and it will be the topic of a forthcoming paper in preparation. The aforementioned analysis of velocity gradients has been also applied to spectroscopic observations of galaxies in the optical band (see e.g. Den Hartog & Katgert 1996; Biviano et al. 1996; Hwang & Lee 2007). A slightly different approach is adopted in Tovmassian (2015), as the rotational state is inferred from the spatial distribution of member galaxies having higher or lower velocities with respect to the mean global velocity. With this criterion 26 per cent of the analysed clusters is found to be rotating. Manolopoulou & Plionis (2016) have recently proposed a variant of the velocity gradients method, identifying rotating clusters from the projection of the velocity of single galaxies along the line of sight. In a total sample of ~ 50 analysed clusters, they find a fraction of 35 per cent rotating candidates with galaxy rotational velocities of the order of thousands of km s^{-1} . A possible comparison of the results from the observational approaches applied to the diffuse gas and those applied to the discrete galaxies, could be a more robust way to establish the presence of a rotation in clusters.

Cosmological N-body simulations are useful tools to characterize in more detail the dynamics within cosmic structures. Mock X-ray signals from simulated clusters have been produced to investigate the indications of a possible

rotation. For example, Roettiger & Flores (2000) simulated a cluster with the same characteristics of Abell 3266, and applied an off-axis merger that produced a rotation associated to bulk flows of about 800 km s^{-1} . The study of the ellipticity of the isophotes in simulated X-ray surface brightness maps has been proposed as another possible way to infer the dynamics of a cluster, as it could be a sign of a rotation (Fang, Humphrey & Buote 2009; Bianconi, Ettori & Nipoti 2013), even if there is not a common agreement (see e.g. Biffi, Dolag & Böhringer 2011). There are different works in literature where the angular momentum properties of large samples of synthetic objects are investigated (e.g. Barnes & Efstathiou 1987; Efstathiou et al. 1988; Bullock et al. 2001; Van den Bosch et al. 2002; Sharma & Steinmetz 2005), mostly with the application to DM haloes. With the improvement of the models adopted to simulate the evolution of gas and astrophysical processes, the ICM dynamics has also been analysed (see e.g. Rasia, Tormen & Moscardini 2004; Faltenbacher et al. 2005; Fang et al. 2009; Lau, Kravtsov & Nagai 2009; Biffi et al. 2011; Lau, Nagai & Nelson 2013), recently also with the prescription for AGN feedback (e.g. in Biffi, Dolag & Böhringer 2013; Nagai et al. 2013). From a statistical analysis of simulated objects, it has emerged that rotational motions seem to predominate in the innermost regions of disturbed clusters rather than in relaxed ones (Biffi et al. 2011), while in outer regions relaxed clusters show a larger contribution from gas rotation instead (Fang et al. 2009; Lau et al. 2009).

In this work we extract for the first time information on spin, angular momentum and velocity properties of ICM and DM in a volume-limited sample of *massive clusters of galaxies* from MUSIC simulations, for which a non-radiative model and two radiative models for gas physics have been used. To this scope we compute the specific angular momentum and the velocity profiles along the cluster radius, also looking for possible correlations between DM and ICM. We adopt in particular a couple of recently proposed models with which we compare the radial profiles of the tangential velocity, that we derive from the specific angular momentum.

This paper is organized as follows. In section 2 we describe the main characteristics of the sample of simulated clusters. In section 3 we perform the analysis of the spin parameter of these clusters. Section 4 is devoted to the description of the radial profiles of the angular momentum of DM and ICM in relaxed clusters and shows the corresponding behaviours. The main results of the analysis of the tangential velocity and its dispersion are presented in section 5, together with a new model that we propose to describe the ICM rotational motions. In section 6 we show the comparison of the angular momentum at virial radius between the DM and gas components. Finally, we summarize our results in section 7.

2 THE DATASET

2.1 MUSIC

The MUSIC¹ dataset is one of the largest catalogues of hydrodynamic simulations of galaxy clusters, with more than 700 clusters and 2000 groups of galaxies (Sembolini et al. 2013). It consists of two sets (named MUSIC-1 and MUSIC-2) of re-simulated objects extracted from two large-volume N-body simulations. In this paper, we focus on the MUSIC-2 sample containing a large statistic of massive objects. The systems were selected from the $(1h^{-1} \text{ Gpc})^3$ volume of the MultiDark simulation (Prada et al. 2012), performed using the best-fitting cosmological parameters from WMAP7+BAO+SNI ($\Omega_m = 0.27$, $\Omega_b = 0.0469$, $\Omega_\Lambda = 0.73$, $\sigma_8 = 0.82$, $n = 0.95$, $h = 0.7$) (Komatsu et al. 2011).

Once the clusters were identified, the zooming technique by Klypin et al. (2001) was adopted to create new initial conditions. These enabled re-simulations at higher mass resolution of the spherical regions around the cluster centres with radii equal to $6h^{-1} \text{ Mpc}$. The new sets were carried out with the parallel TreePM+SPH GADGET-3 code which includes the entropy-conserving implementation of smoothed particle hydrodynamics (SPH) (Springel 2005). Three re-simulation sets were produced accounting for different models to describe the baryon physical processes. We will refer to NR for the non-radiative subset, to CSF for the run including cooling, star-formation and stellar feedback, and to AGN to the simulation that, further, adds the AGN feedback. The DM particle mass is set to $m_{\text{DM}} = 9.0 \times 10^8 h^{-1} M_\odot$, while the gas mass particle is equal to $m_{\text{gas}} = 1.9 \times 10^8 h^{-1} M_\odot$ in the NR set, and it is variable in the radiative simulations. Even in this case, however, m_{gas} is still of the order of $10^8 h^{-1} M_\odot$.

When modelling the sub-grid physics of our CSF and AGN subsets, we accounted for the effects of radiative cooling, UV photoionization, star formation and supernova feedback, including the effects of strong winds from supernovae, as described in the Springel & Hernquist (2003) model. Stars are assumed to form from cold gas clouds on a characteristic timescale t_* , and a stellar mass fraction $\beta = 0.1$ (consistent with assuming an Universal Salpeter IMF with a slope of -1.35) is instantaneously released due to supernovae from massive stars ($M > 8 M_\odot$). In addition to this mass injection of hot gas, thermal energy is also released to the interstellar medium by the supernovae. The number of collisionless star particles spawned from one SPH parent gas particle is fixed to 2. Kinetic feedback is also included: gas mass losses due to galactic winds, \dot{M}_w , is assumed to be proportional to the star formation rate M_{SFR} , i.e. $\dot{M}_w = \eta M_{\text{SFR}}$ with $\eta = 2$. Additionally, the wind contains a fixed fraction $\epsilon = 0.5$ of the total supernova energy. SPH particles near the star formation region are subject to enter in the wind in a stochastic way, given an isotropic velocity kick of $v = 400 \text{ km s}^{-1}$. The simulations including AGN feedback have been carried with the same version of the GADGET-3 code that has been used for the simulations presented in Planelles et al. (2014). This model is based on the original implementation by Springel, Di Matteo & Hernquist (2005) (SMH model), with feedback energy released as a

result of gas accretion onto supermassive black holes (BH). In this AGN model, BHs are described as sink particles, which grow their mass by gas accretion and merging with other BHs. The seeding of BH particles has been modified with respect to the original SMH model, and occurs only in haloes where star formation took place. A minimum mass of $5 \times 10^6 h^{-1} M_\odot$ is assumed for a friends-of-friends (FoF) group of star particles to be seeded with a BH particle. Seeded BHs are located at the potential minimum of the FoF group, instead of at the density maximum, as originally implemented by SMH. The pinning of the BH is regulated at each time-step to avoid advection. In this way a BH particle remains within the host galaxy, when this becomes a satellite of a larger halo. A more strict momentum conservation during gas accretion and BH merger is also set. Two BHs now merge when they are located at a distance from each other that is less than the gravitational softening and when their relative velocity is less than half of the sound speed. Finally, the AGN feedback is provided via thermal energy to the surrounding gas particles. Eddington-limited Bondi accretion produces a radiated energy which corresponds to a fraction $\epsilon_r = 0.1$ of the rest-mass energy of the accreted gas. A fraction of this radiated energy is thermally coupled to the surrounding gas with feedback efficiency $\epsilon_f = 0.1$. This parameter is regulated to reproduce the observed relation between the BH mass and stellar mass of the hosting halo (Ragone-Figueroa et al. 2013). Special care is devoted to the treatment of multi-phase and star forming particles to avoid losing the AGN energy (see Planelles et al. 2014, for details). No mechanical feedback is implemented in these runs, therefore jets and raising bubbles are not described. The transition from a ‘quasar’ phase to a ‘radio’ mode of the BH feedback happens when the accretion rate onto the BH becomes smaller than 1 per cent of the Eddington accretion (see also Sijacki et al. 2007; Fabjan et al. 2010). At that instant, the efficiency of the AGN feedback is enlarged by a factor of 4.

2.2 Selected sample

We analyse 258 simulated massive clusters with virial masses $M_{\text{vir}} > 5 \times 10^{14} h^{-1} M_\odot$ at $z = 0$, extracted from the MUSIC-2 subset. A first reason for the choice of this mass range is that MUSIC-2 is a complete sample in mass: all the massive objects above a given mass threshold (which varies with redshift) formed in the MultiDark parent simulation have been re-simulated. A second reason lies in the fact that we expect that a possible rotation, which here is investigated by means of the properties of the angular momentum, would be more likely observed/measured in the most massive clusters. Each cluster is analysed in the three aforementioned different flavours (NR, CSF and AGN). Clusters in the CSF and NR datasets have been already employed to study SZ scaling relations (Sembolini et al. 2013, 2014) and X-ray properties (Biffi et al. 2014). The reliability of our code was tested in comparison with different gas-dynamical codes to study the consistency between simulated clusters modelled with different numerical and radiative models (see Sembolini et al. 2016a; Elahi et al. 2016; Cui et al. 2016; Sembolini et al. 2016b).

For our analysis we have made a further classification on the basis of the relaxation and the rotation state, as de-

¹ <http://music.ft.uam.es>

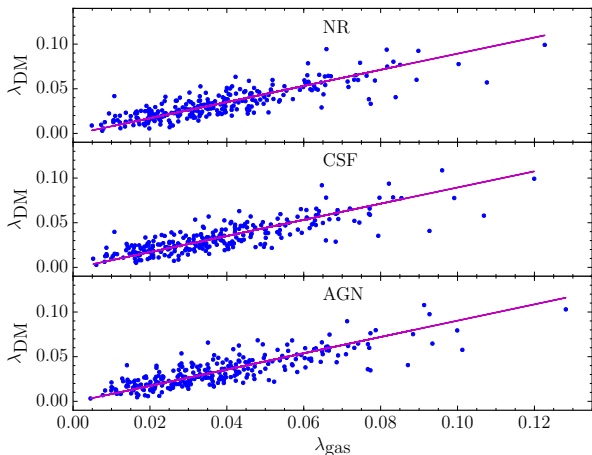


Figure 1. Relation between the spin parameters of the DM and ICM components for all the clusters in the sample. Solid magenta lines represent the robust linear fits.

scribed in detail in section 4. All the useful informations such as particle masses, haloes centre of mass and three-dimensional velocities were retrieved using the Amiga Halo Finder (AHF, Knollmann & Knebe 2009).

3 SPIN PARAMETER ANALYSIS

The rotational state of a halo can be quantified by calculating the spin parameter λ . We adopt the simplified expression from Bullock et al. (2001) derived from the total angular momentum L_{tot} :

$$\lambda_{\text{tot}} = \frac{L_{\text{tot}}}{\sqrt{2}v_{\text{circ}}M_{\text{vir}}R_{\text{vir}}} \quad (1)$$

where v_{circ} indicates the circular velocity as calculated at virial radius, $v_{\text{circ}} = \sqrt{GM_{\text{vir}}/R_{\text{vir}}}$. We remind that other definitions are present in literature (see Peebles 1969; Bullock et al. 2001; Gottlöber & Yepes 2007; Bryan et al. 2013). However, we prefer to use equation(1) for its simplicity, and because we can use it to express the spin parameter of each single matter component (ICM or DM), that we will identify as κ in the following:

$$\lambda_{\kappa} = \frac{L_{\kappa}}{\sqrt{2GM_{\text{vir}}R_{\text{vir}}} M_{\kappa}} \quad (2)$$

(Gottlöber & Yepes 2007). We find that the values of the DM spin parameter are very close to those derived from the total angular momentum. This is not surprising since the mass of the DM component dominates over the baryonic one. The relation between λ_{tot} and λ_{DM} is found to be linear, with a slope close to unity for all the three analysed subsets (NR, CSF and AGN).

In order to explore a possible correlation between the angular momentum of DM and gas, we compare the corresponding spin parameters. A clear linear relation between the two, with a slope $a \sim 0.90$ is shown in Fig. 1, and the full set of parameters obtained from a robust fit to the data using the bisector method (Isobe et al. 1990) is listed in Table 1.

Table 1. Values of the correlation coefficient (c_{corr}) and of the parameters for the linear fits shown in Fig. 1, performed with the bisector method; a indicates the slope, while b indicates the zero-point.

| Dataset | c_{corr} | $a \pm \sigma_a$ | $b \pm \sigma_b$ |
|---------|-------------------|------------------|--------------------|
| NR | 0.84 | 0.90 ± 0.04 | -0.001 ± 0.002 |
| CSF | 0.83 | 0.91 ± 0.05 | -0.001 ± 0.001 |
| AGN | 0.83 | 0.91 ± 0.04 | -0.001 ± 0.001 |

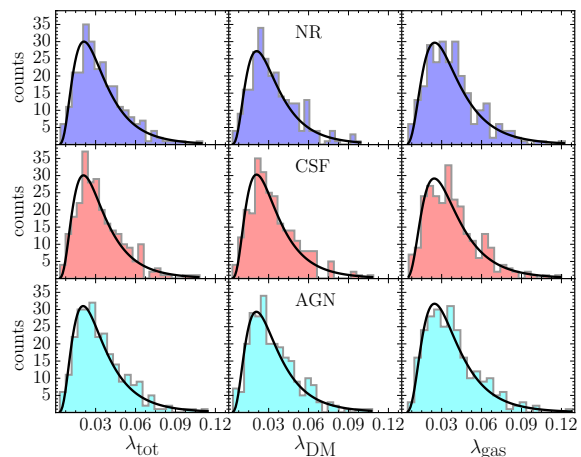


Figure 2. Distributions of the spin parameters of each matter component (along columns) for the three analysed subsets (along rows). Solid lines represent the fits to the lognormal distribution.

Fig. 2 shows the distributions of the spin parameters for gas, DM and total matter components of the clusters in our sample, for the three different flavours. We can see from these results that a lognormal distribution

$$P(\lambda)d\lambda = \frac{1}{\lambda\sqrt{2\pi}\sigma} \exp\left(-\frac{\ln^2(\lambda/\lambda_0)}{2\sigma^2}\right) d\lambda \quad (3)$$

is a valid description of the spin parameters of all the matter components. The scale parameter λ_0 and the shape parameter σ derived from our sample of clusters are reported in Table 2. As expected, the similarity between total and DM values is also evident from these results. When comparing our values of the parameters with other works, (Barnes & Efsthathiou 1987; Bullock et al. 2001; Van den Bosch et al. 2002; Sharma & Steinmetz 2005; Gottlöber & Yepes 2007; Macciò, Dutton & Van den Bosch 2008; Bryan et al. 2013) we find a general agreement. It is worth to stress that these works refer to galactic or proto-galactic haloes, with the exception of Macciò et al. (2008), where objects on different scales are considered (from galaxies to clusters), and of Gottlöber & Yepes (2007), which include clusters of galaxies of the MareNostrum gas-dynamical simulation. Therefore, this result suggests that the shape of the distribution does not vary significantly from galaxies to clusters. The values of $\lambda_{0,\text{gas}}$ are typically larger than those of the DM (by 13 per cent in our case), suggesting more rotational support. This may be because tidal interactions with surrounding large-scale

Table 2. Values of the parameters λ_0 and σ from the lognormal fits to the spin parameter distributions for DM, gas and the total matter components of the analysed sample.

| $\lambda_{0,\text{DM}}$ | σ_{DM} | $\lambda_{0,\text{gas}}$ | σ_{gas} | $\lambda_{0,\text{tot}}$ | σ_{tot} |
|-------------------------|----------------------|--------------------------|-----------------------|--------------------------|-----------------------|
| NR | | | | | |
| 0.0289 | 0.5674 | 0.0333 | 0.5470 | 0.0292 | 0.5655 |
| CSF | | | | | |
| 0.0288 | 0.5638 | 0.0330 | 0.5489 | 0.0287 | 0.5641 |
| AGN | | | | | |
| 0.0289 | 0.5755 | 0.0330 | 0.5416 | 0.0289 | 0.5810 |

structures have had more time to apply torques to the gas accreted at a later time.

4 RADIAL PROFILES OF THE ANGULAR MOMENTUM

After characterizing the spin computed at the virial radius, we move here to study the variations of the specific angular momentum vector along the cluster radius. We produce radial profiles describing of its modulus and orientation with respect to the angular momentum computed at the virial radius. We consider 15 concentric spheres with radius increasing logarithmically, from $r = 0.05R_{\text{vir}}$ to $r = R_{\text{vir}}$. We do not impose any condition on the number of particles in each sphere, but we would like to remark that the minimum amount of particles is always above 10^4 , i.e. enough to lead to robust results. For the i -th sphere, the modulus of the specific angular momentum $j(< r_i) = |\mathbf{j}(< r_i)|$ is estimated as

$$j(< r_i) = \frac{|\mathbf{L}(< r_i)|}{M(< r_i)} = \frac{|\sum_k^{N_i} \mathbf{r}_k \times m_k \mathbf{v}_k|}{\sum_k^{N_i} m_k} \quad (4)$$

where N_i is the number of particles inside the i -th sphere, \mathbf{r}_k is the position of the k -th particle relative to the centre of mass, m_k is its mass, and \mathbf{v}_k is its velocity vector subtracted by the velocity of the centre of mass.

The angle $\alpha(< r_i)$ indicates the variation of the direction of the angular momentum with respect to its orientation at virial radius, and is defined as

$$\alpha(< r_i) = \arccos [\hat{\mathbf{j}}(< r_i) \cdot \hat{\mathbf{j}}(< R_{\text{vir}})] \quad (5)$$

being $\hat{\mathbf{j}}(< r) = \mathbf{j}(< r)/j(< r)$.

In the case of a simple solid body rotation, $\alpha(< r_i)$ is expected to be always null along the cluster radius.

We aim at analysing the coherent rotation of the ICM only in morphologically relaxed clusters, to avoid the influence of outliers in the velocity and in the angular momentum distributions, due to the presence of mergers or of any large substructure within the virial radius. To evaluate the cluster *dynamical state*, we use two of the most adopted indicators present in literature (see e.g. Neto et al. 2007; Power, Knebe & Knollmann 2012; Killedar et al. 2012; Meneghetti et al. 2014; Sembolini et al. 2014; Klypin et al. 2016; Biffi et al. 2016). The first indicator is the spatial offset between the density peak position and the centre of mass position, normalized to the virial radius, $\Delta r = |r_\delta - r_{\text{CM}}|/R_{\text{vir}}$. The

second indicator is the ratio between the mass of the largest substructure within the virial radius, and the cluster virial mass, $M_{\text{sub}}/M_{\text{vir}}$ (see for instance Sembolini et al. 2014, for a more detailed discussion). The assumed threshold values are $\Delta r = 0.10$ for the centre of mass offset, according to D’Onghia & Navarro (2007), and $M_{\text{sub}}/M_{\text{vir}} = 0.10$ for the largest substructure mass to virial mass ratio (Ascibar et al. 2004; Sembolini et al. 2014; Meneghetti et al. 2014). If the values of these indicators are below the respective thresholds, the clusters are classified as relaxed, otherwise they are disturbed and they are not considered in this analysis. With these criteria we select 146 relaxed clusters, corresponding to the 57 per cent of the total sample. This fraction is consistent with results from both observational data (see e.g. Rossetti et al. 2016) and analyses on the morphology of MultiDark simulated clusters (Vega, Yepes & Gottlöber 2016).

To define the *rotational state* of a relaxed cluster we consider the value of the spin parameter of the gas as the discriminant indicator, since it quantifies the contribution of the gas rotational energy to the total energy of the cluster, by definition. We classify a cluster as rotating if it satisfies the condition $\lambda_{\text{gas}} > \lambda_{\text{gas,crit}}$, where $\lambda_{\text{gas,crit}}$ is the threshold that separates the total sample in two sub-samples showing distinguishable profiles of the tangential velocity (see appendix A for details). In our case $\lambda_{\text{gas,crit}} = 0.07$, according to which about 4 per cent of the relaxed cluster sample can be classified as rotating. In separating the population of the relaxed and rotating clusters, the corresponding conditions have been imposed to be valid for all the three subsets (NR, CSF and AGN). In order to verify whether the most massive clusters have the largest rotational support, the correlation between M_{vir} and λ_{gas} has been investigated. Interestingly, we find that the clusters classified as rotating are not the most massive objects in the sample. It is worth to stress, however, that this sample contains all the clusters more massive than $5 \times 10^{14} h^{-1} M_\odot$ that have formed within $(1h^{-1} \text{ Gpc})^3$ volume, with the adopted cosmological model as described in section 2. This leads to an intrinsically limited statistics of objects having large masses, that may contribute in finding a relatively small number of massive rotating clusters.

The ICM mean profiles of $j(< r)$ and $\alpha(< r)$ for the two classes of rotating and non-rotating clusters, are shown in Fig. 3a and Fig. 3b respectively; the profiles for DM are characterized by similar features. Some general trends are evident. On average, the direction of $j(< r)$ reaches more than 60° in the core of non-rotating clusters and it is still above 30° at half of the virial radius. It is also noticeable that several objects register a variation equal and greater than 90° from the core to the outskirts. The rotating clusters show a much smaller variation: for $r \gtrsim 0.3R_{\text{vir}}$ we find that $\alpha(< r)$ is less than $\sim 20^\circ$, pointing out that the orientation is almost fixed. The profiles of the modulus increase from the centre up to the virial radius and flatten in the outskirts, reaching larger values in the rotating clusters, as expected. A similar behaviour has been also found in Bullock et al. (2001), who analysed only the DM component of galaxy-sized haloes. They found a power-law relation of the type $j(< r) \propto r^\beta$ with $\beta = 1.1 \pm 0.3$. In our sample we perform a similar fit to a power-law $j(< r)/j(< R_{\text{vir}}) \propto r^\beta$ to the profiles over spherical shells, normalized at virial radius for

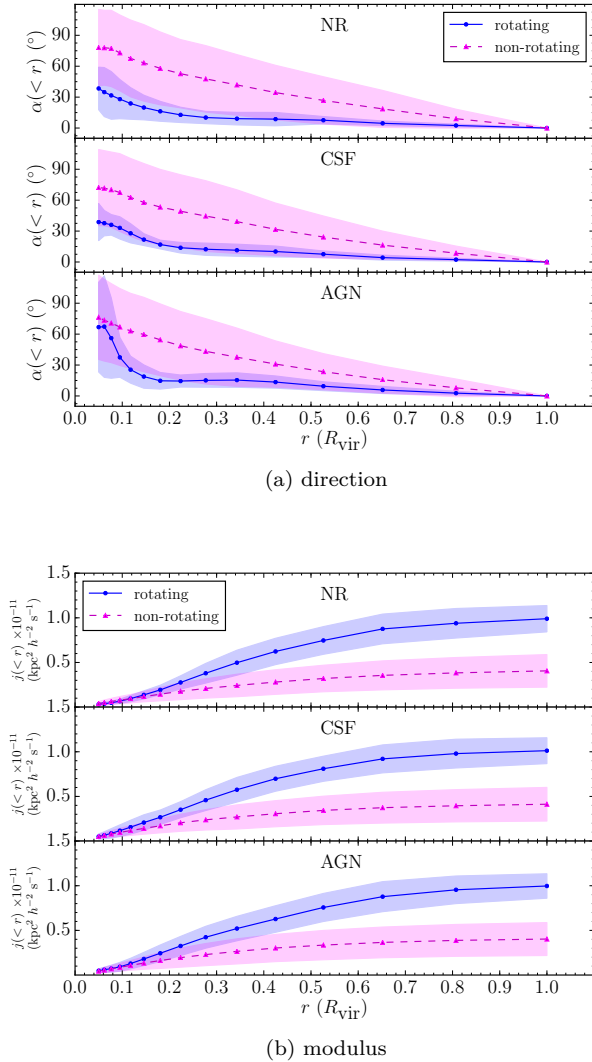


Figure 3. Radial profiles of the orientation (upper panel) and the modulus (lower panel) of the gas specific angular momentum vector for the two populations of relaxed rotating and non-rotating clusters. The points in the plots represent the mean values for each population, and the shaded bands indicate the 1σ scatter with respect to the mean.

Table 3. Mean values and standard deviations of the power-law exponent β as derived from the fits of $j(<r)/j(<R_{\text{vir}})$ for the rotating clusters.

| Dataset | $\beta \pm \sigma_\beta$ | |
|---------|--------------------------|-----------------|
| | gas | DM |
| NR | 0.78 ± 0.13 | 0.96 ± 0.13 |
| CSF | 0.69 ± 0.10 | 0.92 ± 0.15 |
| AGN | 0.75 ± 0.13 | 0.90 ± 0.14 |

the gas and DM components in the rotating clusters. The mean values of β with the corresponding standard deviations are listed in Table 3. The power-law profiles of the DM are in agreement with Bullock et al. (2001), while the values of the gas are 20 per cent lower.

Our results lead to the conclusion that the coherent

rotational motions of ICM and DM in our cluster sample are not properly described by a simple solid body model. A further confirmation of this fact is given by the angles between the angular momentum vector and the three semi-axes describing the ellipsoids that approximate the shape of the matter distribution of gas and DM. Considering only the case of rotating clusters, in fact, these angles range from tens up to 180° , suggesting a misalignment that is not compatible with a rigid rotation.

Finally, we compute $\alpha(<r)$ and $j(<r)$ for the total angular momentum, and comparing the profiles with those obtained for the gas and the DM we found a very close similarity with the latter, reflecting the predominance of this component on the ICM. The dominating role of DM in the cluster dynamics can also be inferred from the lack of significant differences between the results obtained for the three physical flavours of the simulations used to describe the ICM. The only marked difference is the higher average value of gas $\alpha(<r)$, associated with a significant dispersion in the core of the AGN runs ($r < 0.1R_{\text{vir}}$). In this case the AGN feedback likely influences the motion of the gas that, receiving extra energy from the central source, buoyantly raises without any pre-selected orientation. The effect in real clusters might be even more intense for the presence of the AGN jets which are not included in our model.

5 RADIAL PROFILES OF THE VELOCITY

We study the radial profiles of the tangential velocity (or rotational velocity) of gas and DM particles, expressed as:

$$v_{\text{tan}}(r_i) = \frac{\left| \sum_k^{N_i} \frac{\mathbf{r}_k \times m_k \mathbf{v}_k}{|\mathbf{r}_k|} \right|}{\sum_k^{N_i} m_k}, \quad (6)$$

where the sums are extended to the N_i particles located within the 15 spherical shells enclosed between the radii r_{i-1} and r_i , and not to the spheres used above. In this way we get the local values of the tangential velocity, that we use to test possible rotational behaviours. We can derive the tangential velocity from the specific angular momentum, by approximating equation (6) using $v_{\text{tan}}(r_i) \sim \langle |j(r_i)| \rangle / r_i$. In the second term, the contribution from random turbulence motions is averagely null by definition (Ascasibar et al. 2004), thus the average angular momentum computed in a given shell considers only the contribution from rotational coherent motions.

The velocity component associated to macroscopic random motions will be referred hereafter as turbulence, denoted with v_{turb} . We quantify it from the dispersion with respect to the average tangential velocity as in equation (6):

$$v_{\text{turb}}(r_i) = \left[\sum_k^{N_i} m_k \left(\frac{|\mathbf{r}_k \times \mathbf{v}_k|}{|\mathbf{r}_k|} - v_{\text{tan}}(r_i) \right)^2 / \sum_k^{N_i} m_k \right]^{\frac{1}{2}}, \quad (7)$$

where the sums are extended also here to spherical shells for gas and DM particles.

Both velocity profiles (equations (6) and (7)) are normalized to the circular velocity v_{circ} of the corresponding cluster at R_{vir} . In our sample we have an average value of

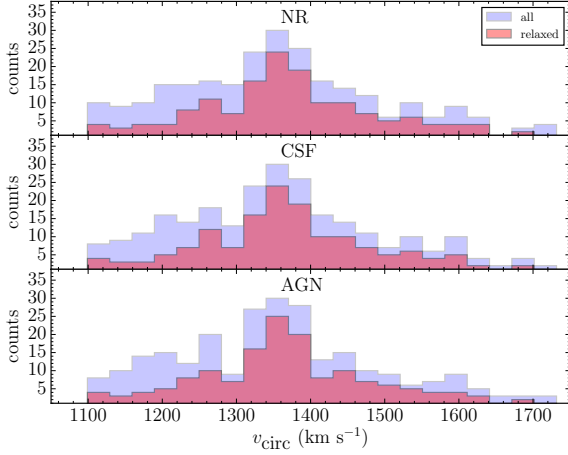


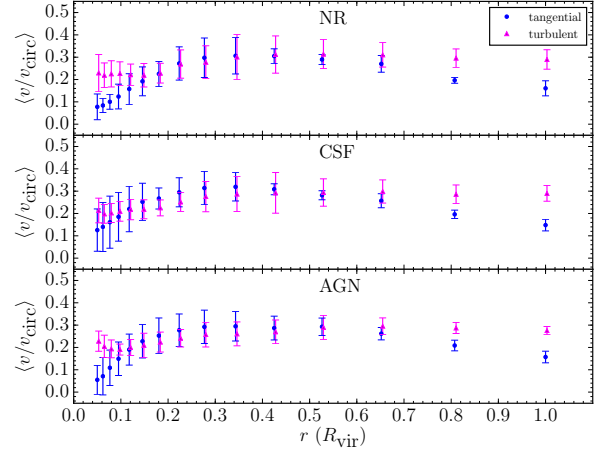
Figure 4. Distribution of the circular velocity as calculated at the virial radius for the clusters in the analysed sample, with the discrimination of the relaxed ones.

$\langle v_{\text{circ}} \rangle = (1365 \pm 145) \text{ km s}^{-1}$. The distribution is shown in Fig. 4. Due to the tight correlation between the total mass and the circular velocity (Evrard et al. 2008), these distributions emphasize that there is no mass segregation for relaxed clusters.

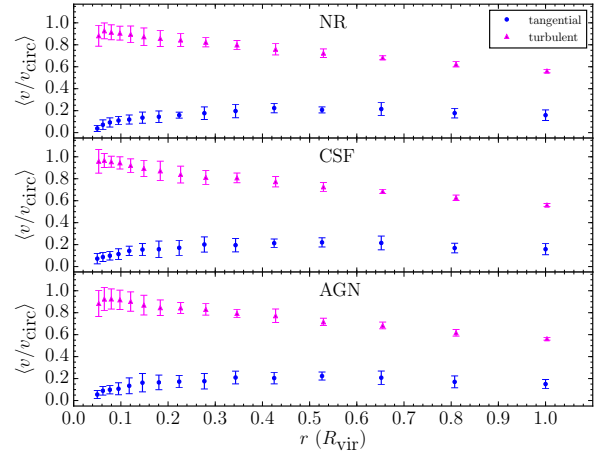
The mean profiles of the tangential and turbulent velocity have been calculated for both classes of clusters (rotating and non-rotating) introduced in section 4, for all the physical flavours. Since the tangential velocity is derived from the specific angular momentum, whose direction changes significantly along the radius (Fig. 3a), we multiply its values by the cosine of the mean angle $\alpha(r)$, in the central region ($r < 0.3R_{\text{vir}}$). In this way we fix the orientation, and assume the same rotational plane.

By comparing the radial profiles of the mean tangential and turbulent velocity for the rotating clusters, as shown in Fig. 5a for the ICM and in Fig. 5b for the DM, we find a significant difference between these two matter components. For the DM there is a net distinction between the two velocities: the turbulent velocity dominates over the tangential one, with a decrease of ~ 30 per cent from the centre to the outskirts. In the profiles of ICM velocities instead, there is a comparable contribution from turbulence and coherent rotation in the region between ~ 0.15 and $\sim 0.65R_{\text{vir}}$. Turbulence is still dominant in the innermost and in the outer regions, with a tendency to increase for radial values between 0.1 and $0.4R_{\text{vir}}$, and a flattening for higher radii. Along the whole radial range, values vary between 0.2 and $0.3v_{\text{circ}}$, corresponding to ~ 273 and $\sim 410 \text{ km s}^{-1}$. The larger values of the DM velocity dispersion with respect to the gas can be explained in terms of the absence of radiative mechanisms that remove kinetic energy of particles transforming it into thermal energy, as in the case of gas particles.

From the comparison of our profiles of the velocity dispersion with other works, we find a general consistency. In particular there is a fairly good agreement for the DM profiles, that typically show a decreasing trend and have larger values with respect to the gas (see Sunyaev et al. 2003; Rasia et al. 2004; Faltenbacher et al. 2005). A remarkable agree-



(a) gas

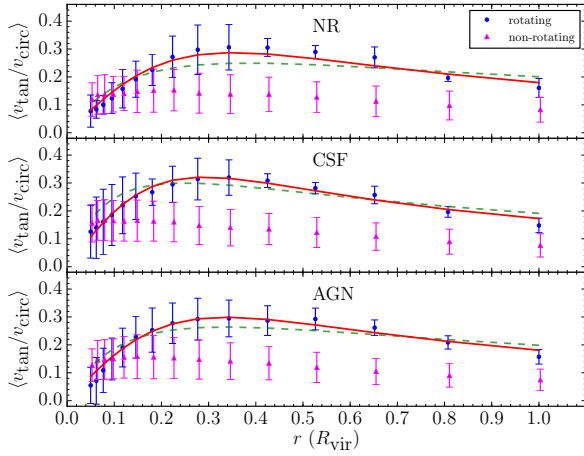


(b) DM

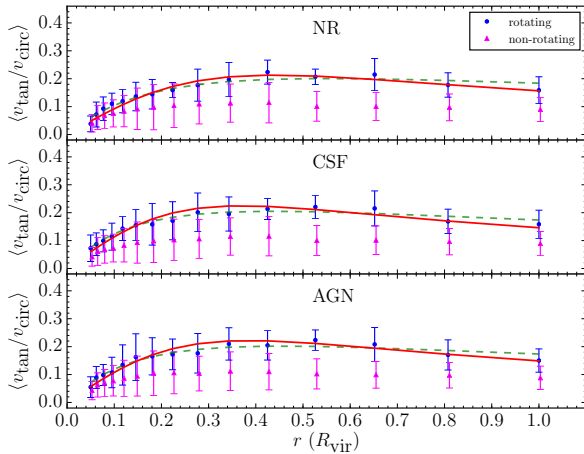
Figure 5. Radial profiles of the mean tangential and turbulent velocity of ICM (upper panel) and DM (lower panel) for the rotating clusters only. The error bars indicate the standard deviation of the single profiles with respect to the mean profiles.

ment can be found with Ascasibar et al. (2004), as the values are compatible within the errors over all the considered radial range. Values are generally around a thousand of km s^{-1} in the central regions, and differ more significantly in the outskirts.

The profiles of ICM turbulence show less regular behaviours. A recurring trend is the flattening for radii $r \gtrsim 0.75R_{\text{vir}}$, and values typically span a relatively narrow range. In particular our values are compatible with Faltenbacher et al. (2005) in the innermost regions ($r \sim 0.10R_{\text{vir}}$), and with Rasia et al. (2004) and Lau et al. (2009) at intermediate radii. The agreement with the latter is of particular interest, as they take into account the dynamical state of the clusters, thus only the profiles of the relaxed ones have been compared here. We find more marked differences with Sunyaev et al. (2003), possibly because only a cluster is considered in their analysis, thus they are more sensitive to single-cluster properties.



(a) gas



(b) DM

Figure 6. Radial profiles of the mean rotational velocity of ICM (upper panel) and DM (lower panel) for the rotating and the non-rotating clusters. The error bars indicate the standard deviation of the single profiles with respect to the mean profiles. The dashed green line is the fit with the vp2 model, while the red solid line is the fit to the model of equation (10) (see text).

The radial profiles of the tangential velocity for the rotating and the non-rotating clusters are shown in Fig. 6a and in Fig. 6b, for the ICM and the DM respectively. Differently from the case of the turbulent velocity profiles, there is a common trend for both the gas and the DM, consisting in the increase of the values in the innermost regions up to $0.3 - 0.4R_{\text{vir}}$, where they reach $\sim 400 \text{ km s}^{-1}$ for the ICM and $\sim 250 \text{ km s}^{-1}$ for the DM, and a smooth decrease in the outskirts. Values at virial radius are around 16 per cent of the circular velocity in the rotating clusters, and 8 per cent in the non-rotating clusters (with no substantial differences between ICM and DM). These results are in fairly good agreement with the values reported in [Ascasibar et al. \(2004\)](#) for the DM and in [Lau et al. \(2009\)](#) for the gas. The plots in Fig. 6 clearly show that single profiles are affected

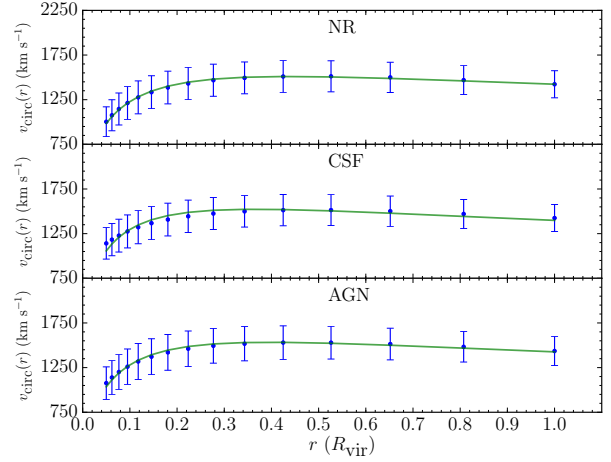


Figure 7. Circular velocity estimated inside spheres with increasing radius, averaged over all the clusters with 1σ dispersion. The green solid line is the fit to the vp1 model of equation (8).

by relatively large scatters, because of the different intrinsic behaviours of individual clusters.

In order to check whether our mean profiles of the tangential velocity can be described by an analytical rotational model, we fit them to the two models introduced by [Bianconi et al. \(2013\)](#). We neglected the simple solid body model, since we can see from the angular momentum profiles shown in section 4 that it is not appropriate to describe the rotational motions in our cluster sample. The two models that we consider refer to the case of a non-rigid rotating ICM, whose contribution to the gravitational potential of the cluster is negligible. The first proposed model, referred hereafter as vp1, is the circular velocity of the gas in a Navarro-Frenk-White (NFW) DM density distribution ([Navarro, Frenk & White 1997](#)), as a function of the radial distance from the centre:

$$v_{\text{circ}}(r) = v_{c0} \left[\frac{\ln(1+r/r_0)}{r/r_0} - \frac{1}{1+r/r_0} \right]^{\frac{1}{2}}, \quad (8)$$

where the radius r_0 corresponds to the peak value of the velocity. Since it represents the circular velocity along the cluster radius, this profile is not fully appropriate to fit our tangential velocity. Therefore we fit to vp1 the profile of the circular velocity computed over different radial spheres, $v_{\text{circ}}(r) = \sqrt{GM(r)/r}$, and we find a very good agreement, as shown in Fig. 7. The second model proposed by [Bianconi et al. \(2013\)](#) is an alternative to the circular velocity profile, characterized by a steeper increase in the core regions and a deeper decrease in the outskirts:

$$v_{\text{tan}}(r) = v_{t0} \frac{r/r_0}{(1+r/r_0)^2} \quad (9)$$

that will be referred hereafter as vp2 model. We also introduce a modified version of vp2, the vp2b model, of equation:

$$v_{\text{tan}}(r) = v_{t0} \frac{r/r_0}{1+(r/r_0)^2}. \quad (10)$$

The fits of the mean tangential velocity profiles to the vp2

Table 4. Parameters of the fit with the vp2 (equation (9)) and vp2b (equation (10)) models of the mean tangential velocity of gas and DM for rotating clusters.

| Dataset | $(v_{t0} \pm \sigma_{v_{t0}})$ (v_{circ}) | $(r_0 \pm \sigma_{r_0})$ (R_{vir}) |
|----------|--|---|
| gas vp2 | | |
| NR | 1.00 ± 0.04 | 0.38 ± 0.05 |
| CSF | 1.21 ± 0.07 | 0.24 ± 0.04 |
| AGN | 1.07 ± 0.07 | 0.33 ± 0.05 |
| DM vp2 | | |
| NR | 0.80 ± 0.06 | 0.55 ± 0.12 |
| CSF | 0.82 ± 0.07 | 0.44 ± 0.09 |
| AGN | 0.81 ± 0.07 | 0.45 ± 0.10 |
| gas vp2b | | |
| NR | 0.58 ± 0.03 | 0.35 ± 0.03 |
| CSF | 0.65 ± 0.04 | 0.29 ± 0.03 |
| AGN | 0.60 ± 0.04 | 0.33 ± 0.04 |
| DM vp2b | | |
| NR | 0.42 ± 0.03 | 0.44 ± 0.06 |
| CSF | 0.45 ± 0.03 | 0.37 ± 0.05 |
| AGN | 0.44 ± 0.04 | 0.38 ± 0.06 |

and vp2b models can be seen in Fig. 6a for the gas and in Fig. 6b for the DM. The v_{t0} and r_0 parameters which best fit equations (9) and (10) are listed in Table 4. Both models are in agreement with the data within one standard deviation; the residuals are lower for the vp2b, that better fits the ICM data, especially around the bump observed at $r \sim 0.3R_{\text{vir}}$ and in the external regions. The similar behaviours of gas and DM suggest a co-rotation of these two components, that is further investigated in section 6.

6 CO-ROTATION OF THE DM AND THE ICM

We drop here the distinction between relaxed and unrelaxed clusters, and we focus on the specific angular momentum vectors of gas (\mathbf{j}_{gas}) and DM (\mathbf{j}_{DM}) at virial radius, aiming at exploring possible correlations between the two components. In particular we compare the orientation and the absolute value of these two vectors. Using the direction vectors, $\hat{j}_{\text{gas}} = \mathbf{j}_{\text{gas}}/j_{\text{gas}}$ and $\hat{j}_{\text{DM}} = \mathbf{j}_{\text{DM}}/j_{\text{DM}}$ (being $j_{\text{gas}} = |\mathbf{j}_{\text{gas}}|$ and $j_{\text{DM}} = |\mathbf{j}_{\text{DM}}|$), the angle between the two angular momenta at virial radius is computed as

$$\theta_{\text{gas,DM}} = \arccos [\hat{j}_{\text{gas}}(R_{\text{vir}}) \cdot \hat{j}_{\text{DM}}(R_{\text{vir}})] . \quad (11)$$

For our goal, we consider that two vectors are aligned if $\theta_{\text{gas,DM}} < 10^\circ$. Under this condition the gas and DM particles are co-rotating, and the motions of DM could be inferred by measuring the gas.

The distribution of $\theta_{\text{gas,DM}}$ for all the clusters in the sample is reported in Fig. 8. Around 40 per cent of the sample (corresponding to ~ 100 objects) shows $\theta_{\text{gas,DM}} < 10^\circ$. In Fig. 9 we plot the angle $\theta_{\text{gas,DM}}$ as a function of λ_{gas} , discriminating by the relaxation state of the clusters. We find that the dynamical state does not seem to play a relevant role on the alignment between gas and DM. The values of $\theta_{\text{gas,DM}}$ are below 20° for relatively high values of λ_{gas} . In the clusters classified as rotating (having $\lambda_{\text{gas}} > 0.07$) the angle values are about 10° . This leads to the conclusion that a larger cluster rotation is linked to a larger alignment of the angular momenta of gas and DM. Such alignment can be seen as the evidence for a co-rotation of these two

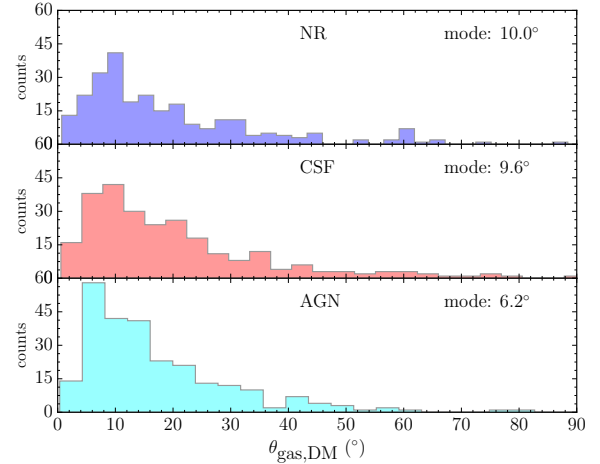


Figure 8. Distributions of the angles between gas and DM angular momenta at virial radius. For $\theta_{\text{gas,DM}} > 90^\circ$ there are only few isolated clusters.

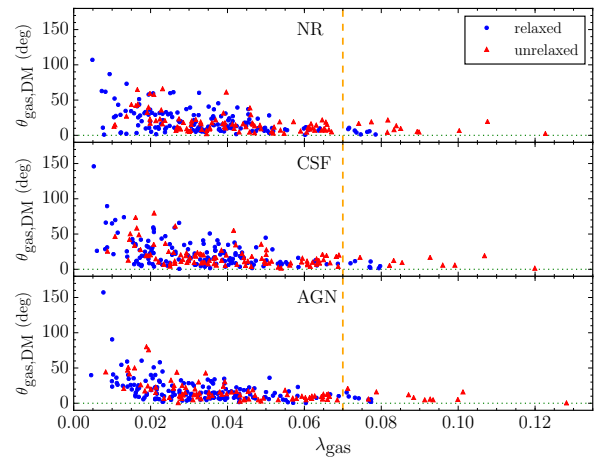


Figure 9. Angle $\theta_{\text{gas,DM}}$ versus the spin parameter of the gas, with the distinction for relaxed and unrelaxed clusters. The dashed orange line indicates the threshold value for the separation of the rotating clusters from the non-rotating ones.

components, considering that the orientation of the angular momentum for radial values $r \gtrsim 0.3R_{\text{vir}}$ (see Fig. 3a) is almost fixed.

As in the case of the orientation, we also expect a correlation in the absolute values of the angular momentum of the two components. Fig. 10 shows the relation between $j_{\text{gas}}(R_{\text{vir}})$ and $j_{\text{DM}}(R_{\text{vir}})$ for our dataset. A correlation between the absolute values is present, and the parameters of the linear fits to the data performed with the bisector method are listed in Table 5. It is worth noting that the slope value of ~ 0.94 is consistent within the error with the value obtained from the correlation between the spin parameters of the DM and gas component (see Table 1). From this result we find that the ICM specific angular momentum is a factor of ~ 1.06 larger than that of DM. However, we also find that

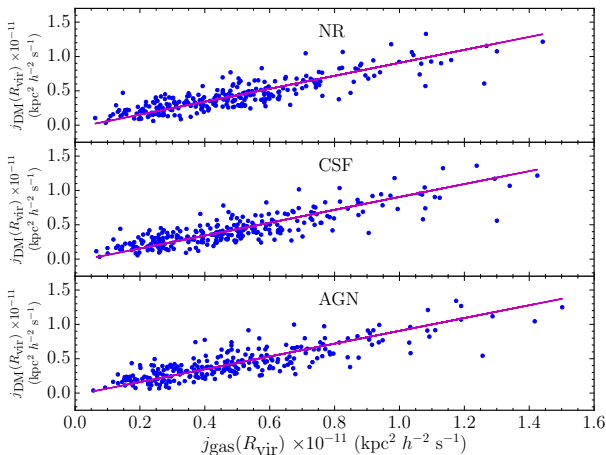


Figure 10. Relation between the absolute values of the specific angular momentum of DM and gas at virial radius; robust linear fits are also shown.

Table 5. Parameters of the robust linear fits performed on the $j_{\text{DM}}(R_{\text{vir}})$ vs $j_{\text{gas}}(R_{\text{vir}})$ plots. a and b are the slope and the zero-point respectively; c_{corr} indicates the correlation coefficient.

| Dataset | c_{corr} | $a \pm \sigma_a$ | $b \pm \sigma_b$ ($\text{kpc}^2 h^{-2} \text{s}^{-1}$) |
|---------|-------------------|------------------|--|
| NR | 0.85 | 0.94 ± 0.04 | $(-4 \pm 2) \times 10^{-13}$ |
| CSF | 0.84 | 0.94 ± 0.04 | $(-3 \pm 2) \times 10^{-13}$ |
| AGN | 0.83 | 0.93 ± 0.04 | $(-3 \pm 2) \times 10^{-13}$ |

the gas angular momentum fraction $\ell_{\text{gas}} = L_{\text{gas}}/L_{\text{DM}} \sim 0.17$ at virial radius, meaning that when masses are taken into account, the DM contribution to the angular momentum is dominant.

7 SUMMARY AND CONCLUSIONS

In this work we have investigated the presence of rotational motions in the most massive clusters of MUSIC-2, a large dataset of gas-dynamical simulations. We considered different physical models to describe the ICM: radiative and non-radiative, with and without AGN feedback. We focused on the study of the specific angular momentum and of the tangential and random velocity components. We have selected only the relaxed clusters, avoiding the impact of merging processes and/or large substructures motions, which enlarge the contribution of turbulence. We discriminate the rotating haloes through the value of the spin parameter of the gas. It must be remarked that the threshold value that has been adopted is relatively high, in order to take into account objects with a large rotational support. This contributes in having a relatively low statistics of clusters classified as rotating.

The main results of this analysis can be summarized as follows.

- In general, we find that the results are independent on the models to describe the ICM properties (NR, CSF and AGN). This can be explained by the fact that the dynamics of clusters are dominated by the DM component;

- the spin parameter distributions for gas and DM in our sample of massive simulated clusters are consistent with previous results in literature;

- with the adopted criterion to discriminate the rotational state, we have 4 per cent of the relaxed clusters classified as rotating. The profiles of the specific angular momentum vector for ICM and DM along different radial distances from the centre, averaged over the aforementioned classes, show an almost constant orientation for the rotating clusters at radial distances larger than $0.3R_{\text{vir}}$. The modulus of the specific angular momentum vector increases following a power-law behaviour with exponent $\beta \sim 0.7$ for gas and $\beta \sim 1$ for DM, with the tendency to flatten in the outskirts. All these results lead to the conclusion that a solid body rotation model would not be correct for our clusters;

- the average profiles of the tangential velocity show that the rotational support is small relative to the circular velocity at virial radius (~ 16 per cent for the rotating clusters), but yet non-zero. The velocity dispersion generally dominates, especially for DM. The behaviour of the tangential velocity profile of the rotating clusters, can be modelled with a simple modification of the circular velocity profile derived from the NFW dark matter density distribution in the haloes;

- in a non-negligible fraction of clusters (~ 40 per cent of the total sample) there is evidence for a common behaviour of the DM and the gas components, since their specific angular momenta are correlated both in direction and in modulus. This indicates a possible co-rotation, that is suggested also by the comparison of the behaviour of the radial profiles.

The proof of DM and ICM co-rotation is one of the key results of this study as it can lead to the possibility of inferring DM motions by studying gas motions. They are definitely challenging to measure, however a variety of observational techniques at different wavelengths can be used. Among these, X-ray spectroscopy (or surface brightness mapping) and SZ mapping are the most promising. In particular, instruments with high angular resolutions are necessary for both the production of maps of the kinematic SZ effect towards clusters at a frequency around 200 GHz, and spectroscopic measurements on emission lines from heavy elements in the ICM. The NIKA2 camera at the IRAM 30-m telescope (Monfardini et al. 2014) and the *Athena* satellite (Barcons et al. 2015) respectively, could satisfy these requirements.

In a companion paper we produce synthetic maps of kinematic SZ effect, with which it is possible to map the velocities along the line of sight, and to determine the presence of a rotational motion, if any. We also plan to investigate the correlation between the dynamical properties of ICM and galaxies in our sample, in order to compare the results with the study of cluster rotation inferred from the velocity of galaxies. In particular we aim to apply the analysis developed in Manolopoulou & Plionis (2016) to our sample of clusters to study possible correlations.

ACKNOWLEDGEMENTS

The authors thank the anonymous referee for the constructive comments on the text. They also want to thank Veron-

ica Biffi, Stefano Borgani, Giuseppe Murante and Susanna Planelles for their contribution to the implementation of the code for the run with the AGN feedback and for their comments and suggestions. The MUSIC simulations have been performed in the Marenostrum supercomputer at the Barcelona Supercomputing Centre, thanks to the computing time awarded by Red Española de Supercomputación. This work has been partially supported by funding from Sapienza University of Rome - Progetti di Ricerca Anno 2014 prot. C26A14KYYJ and Anno 2015 prot. C26A15LXNR. GY and FS acknowledge financial support from MINECO (Spain) under research grants AYA2012-31101 and AYA2015-63810-P. ER is financially supported by PIIF-GA-2013-627474 and NSF AST-1210973.

References

Ade P., et al., 2016, *A&A*, 594, A24
 Aharonian F., et al., 2016, *Nature*, 535, 117
 Ascasibar Y., et al., 2004, *MNRAS*, 352, 1109
 Barcons X., et al., 2015, *JPhCS*, 610, 012008
 Barnes J., Efstathiou G., 1987, *ApJ*, 319, 575
 Bianconi M., Ettori S., Nipoti C., 2013, *MNRAS*, 434, 1565
 Biffi V., Dolag K., Böhringer H., 2011, *MNRAS*, 413, 573
 Biffi V., Dolag K., Böhringer H., 2013, *MNRAS*, 428, 1395
 Biffi V., et al., 2014, *MNRAS*, 439, 588
 Biffi V., et al., 2016, *ApJ*, 827, 112
 Biviano A., et al., 1996, *A&A*, 311, 95
 Bryan S. E., et al., 2013, *MNRAS*, 429, 3316
 Bullock J. S., et al., 2001, *ApJ*, 555, 240
 Catelan P., Theuns T., 1996, *MNRAS*, 282, 436
 Chluba J., Mannheim K., 2002, *A&A*, 396, 419
 Cooray A., Chen X., 2002, *ApJ*, 573, 43
 Cui W., et al., 2016, *MNRAS*, 458, 4052
 D’Onglia E., Navarro J. F., 2007, *MNRAS*, 380, L58
 Den Hartog R., Katgert P., 1996, *MNRAS*, 279, 349
 Dupke R. A., Bregman J. N., 2001, *ApJ*, 547, 705
 Efstathiou G., et al., 1988, *MNRAS*, 235, 715
 Elahi P. J., et al., 2016, *MNRAS*, 458, 1096
 Evrard A. E., et al., 2008, *ApJ*, 672, 122
 Fabjan D., et al., 2010, *MNRAS*, 401, 1670
 Faltenbacher A., et al., 2005, *MNRAS*, 358, 139
 Fang T., Humphrey P., Buote D., 2009, *ApJ*, 691, 1648
 Gottlöber S., Yepes G., 2007, *ApJ*, 664, 117
 Hwang H. S., Lee M. G., 2007, *ApJ*, 662, 236
 Isobe T., et al., 1990, *ApJ*, 364, 104
 Killedar M., et al., 2012, *MNRAS*, 427, 533
 Klypin A., et al., 2001, *ApJ*, 554, 903
 Klypin A., et al., 2016, *MNRAS*, 457, 4340
 Knollmann S. R., Knebe A., 2009, *ApJS*, 182, 608
 Komatsu E., et al., 2011, *ApJS*, 192, 18
 Lau E. T., Kravtsov A. V., Nagai D., 2009, *ApJ*, 705, 1129
 Lau E. T., Nagai D., Nelson K., 2013, *ApJ*, 777, 151
 Liu A., et al., 2015, *ApJ*, 809, 27
 Liu A., et al., 2016, *ApJ*, 821, 29
 Macciò A. V., Dutton A. A., Van den Bosch F. C., 2008, *MNRAS*, 391, 1940
 Manolopoulou M., Plionis M., 2016, preprint (arXiv:1604.06256)
 Meneghetti M., et al., 2014, *ApJ*, 797, 34
 Monfardini A., et al., 2014, *JLTP*, 176, 787
 Nagai D., et al., 2013, *ApJ*, 777, 137
 Navarro J., Frenk C. S., White S. D. M., 1997, *ApJ*, 490, 493
 Neto A. F., et al., 2007, *MNRAS*, 381, 1450
 Nipoti C., et al., 2015, *JPIPh*, 81, 495810508
 Peebles P. J. E., 1969, *ApJ*, 155, 393

Planelles S., et al., 2014, *MNRAS*, 438, 195
 Power C., Knebe A., Knollmann S. R., 2012, *MNRAS*, 419, 1576
 Prada F., et al., 2012, *MNRAS*, 423, 3018
 Ragone-Figueroa C., et al., 2013, *MNRAS*, 436, 1750
 Rasia E., Tormen G., Moscardini L., 2004, *MNRAS*, 351, 237
 Ricker P. M., 1998, *ApJ*, 496, 670
 Ricker P. M., Sarazin C. L., 2001, *ApJ*, 561, 621
 Roettiger K., Flores R., 2000, *ApJ*, 538, 92
 Rossetti M., et al., 2016, *MNRAS*, 457, 4515
 Sembolini F., et al., 2013, *MNRAS*, 429, 323
 Sembolini F., et al., 2014, *MNRAS*, 440, 3520
 Sembolini F., et al., 2016a, *MNRAS*, 457, 4063
 Sembolini F., et al., 2016b, *MNRAS*, 459, 2973
 Sharma S., Steinmetz M., 2005, *ApJ*, 628, 21
 Sijacki D., et al., 2007, *MNRAS*, 380, 877
 Springel V., 2005, *MNRAS*, 364, 1105
 Springel V., Hernquist L., 2003, *MNRAS*, 339, 289
 Springel V., Di Matteo T., Hernquist L., 2005, *MNRAS*, 361, 776
 Sunyaev R. A., Norman M. L., Bryan G. L., 2003, *AstL*, 29, 783
 Tovmassian H. M., 2015, *Ap*, 58, 328
 Tutukov A. V., Dryomov V. V., Dryomova G. N., 2007, *ARep*, 51, 435
 Van den Bosch F. C., et al., 2002, *ApJ*, 576, 21
 Vega J., Yepes G., Gottlöber S., 2016, preprint (arXiv:1603.02256)
 Vikhlinin A., et al., 2009, *ApJ*, 692, 1060

APPENDIX A: CRITICAL VALUE OF THE GAS SPIN PARAMETER FOR ROTATING CLUSTERS

Since there is not a universal critical value for λ_{gas} that can be adopted to discriminate rotating objects, we choose the threshold by inspecting the radial average profiles of the tangential velocity (see the detailed description in section 5) of the two populations of rotating and non-rotating clusters, ($v_{\text{tan}}^{\text{rot}}(r)$ and $v_{\text{tan}}^{\text{nonrot}}(r)$, respectively). We take the value for which these profiles are separated more than the corresponding standard deviations over $r \gtrsim 0.3R_{\text{vir}}$, that is the radial range where the angular momentum orientation is almost fixed (see section 4). To quantify the separation of the profiles at a radius r , indicating with $\sigma_{\text{tan}}^{\text{rot}}(r)$ and $\sigma_{\text{tan}}^{\text{nonrot}}(r)$ the corresponding standard deviations (represented by the error bars in the profile plots), we introduce the following estimator

$$d_v(r) = \frac{|v_{\text{tan}}^{\text{rot}}(r) - v_{\text{tan}}^{\text{nonrot}}(r)|}{\sigma_{\text{tan}}^{\text{rot}}(r) + \sigma_{\text{tan}}^{\text{nonrot}}(r)}, \tag{A1}$$

so that they can be considered as separated when $d_v(r) > 1$. The best $\lambda_{\text{gas,crit}}$ is the one for which the minimum value of $d_v(r)$, d_{vm} , is larger than one in the range $r \gtrsim 0.3R_{\text{vir}}$. The fraction of relaxed clusters which, according to our criterion, can be defined as rotating is listed in Table A1 for some values of $\lambda_{\text{gas,crit}}$, together with d_{vm} . It results that the $\lambda_{\text{gas,crit}}$ having $d_{vm} > 1$ in the chosen radial range is 0.07, therefore we adopt this value as the discriminating one. Fig. A1 shows the profiles for $\lambda_{\text{gas,crit}} = 0.03$, where the overlapping of the two classes for $r \lesssim 0.5R_{\text{vir}}$ is evident. Values of $\lambda_{\text{gas,crit}}$ larger than 0.07 cannot be tested, since the maximum spin parameter of the gas in the sub-sample of relaxed clusters is ~ 0.078 . From Fig. 2 it can be seen that these values correspond to the tails of the spin parameter distributions.

Table A1. Threshold values for the gas spin parameter and corresponding percentage of rotating clusters with respect to the number of relaxed clusters, $N_{\text{rot}}/N_{\text{rel}}$. The d_{vm} value is also shown (see text).

| $\lambda_{\text{gas,crit}}$ | $N_{\text{rot}}/N_{\text{rel}}$ | d_{vm} |
|-----------------------------|---------------------------------|----------|
| 0.03 | 49% | 0.49 |
| 0.05 | 10% | 0.85 |
| 0.07 | 4% | 1.11 |

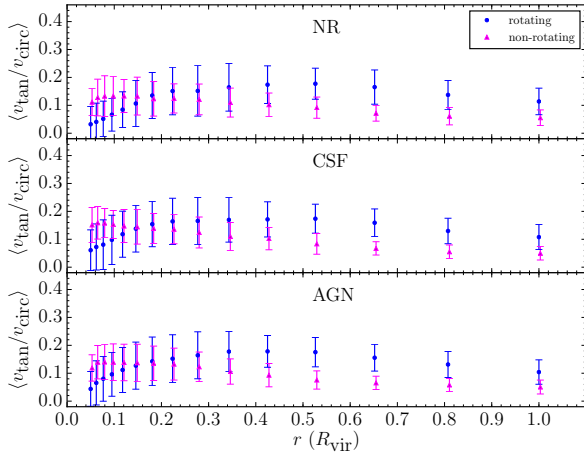


Figure A1. Radial profiles of the tangential velocity of the gas for the rotating and the non-rotating clusters, assuming $\lambda_{\text{gas,crit}} = 0.03$. See the caption of Fig. 6 for a detailed description of the plots.

This paper has been typeset from a $\text{\TeX}/\text{\LaTeX}$ file prepared by the author.